The Meteoritical Society

Meteoritics & Planetary Science 1–10 (2021)
doi: 10.1111/maps.13752

Revisiting the Wasson fractional crystallization model for IIIAB iron meteorites with implications for the interpretation of their Fe isotope ratios

Edward D. YOUNG*

Department of Earth, Planetary, and Space Sciences, University of California, Los Angeles, California 90095, USA
*Corresponding author. E-mail: eyoung@epss.ucla.edu

(*Received 11 March 2021; revision accepted 04 September 2021*)

Abstract–The trapped melt fractional crystallization model for the IIIAB iron meteorites put forward by J. T. Wasson two decades prior is revisited. The basic precepts upon which the model was based remain true, and the model can be implemented using Ir and Au solid/liquid distribution coefficients that are broadly consistent with experimental data. For this reason, the difference between the Wasson model and some more recent trapped melt models lies mainly with inferences about the S concentrations of the core of the IIIAB iron meteorite parent body. For the Wasson model, S bulk concentrations of about 2 wt% are implied. For the more recent model, much greater concentrations of between about 12–15 wt% are indicated. The two different trapped melt models profoundly influence the interpretation of high δ^{57}Fe values relative to chondrites in the IIIAB irons. The Wasson model suggests that there should be more variations in δ^{57}Fe than are observed among these meteorites, while the more recent trapped melt model relies on the crystallization of FeS from the trapped melt to raise the δ^{57}Fe of the latter, thus minimizing the variability. The interpretation of Fe isotope ratios in the IIIAB meteorites therefore depends critically on the S concentration of the parent body core.

INTRODUCTION

Magmatic iron meteorites represent the fragments of the cores of differentiated planetesimals formed early in the history of the solar system. They therefore provide unparalleled information about the formation and evolution of metal cores that are otherwise inaccessible (Lovering, 1957). Scott (1977) articulated the concept that the range in elemental abundances in the IIIAB group of iron meteorites is indicative of fractional crystallization of the parent body metallic core using in part linear trends on log–log plots of elemental concentrations. Wasson (1999), building on earlier work (e.g., Esbensen et al., 1982), proposed a fractional crystallization and trapped melt model for the compositional variability among IIIAB iron meteorites. Here, we review the basis for this model. The goal is to recall that the trends defined by the IIIAB trace element data are consistent with the most basic principles of fractional crystallization, and that remnants of both solids and liquids are evidently preserved among the IIIAB meteorites. This brief review is timely in that the separation of solids and melts evidenced in the IIIAB meteorites has important implications for the interpretations of their iron isotope ratios. The IIIAB irons are enriched in heavy Fe isotope ratios, with elevated δ^{57}Fe values (per mil deviations in ^{57}Fe/^{54}Fe) with an average of approximately 0.13½ relative to chondrites (Chernonozhkin et al., 2016; Jordan et al., 2019; Kehm et al., 2003; Poitrasson et al., 2004; Schoenberg & von Blanckenburg, 2006; Weyer et al., 2005; Williams et al., 2006; Zhu et al., 2002). This is puzzling because the vast majority of the iron in a differentiated planetesimal should reside in the metallic core, and if the parent bodies were formed ultimately by accretion of chondrite-like bodies, or by accretion of bodies with isotope ratios similar to chondrites, as seems likely, one would expect δ^{57}Fe of the core material to be approximately chondritic. Fractionation of Fe isotopes between solid and liquid Fe-rich metal is a possible mechanism for Fe isotope fractionation among magmatic iron meteorites. Ni et al. (2020)

showed that solid metal in the Fe-Ni-S system favors ^{57}Fe over ^{54}Fe relative to coexisting molten metal by up to 0.2‰ at relevant temperatures, suggesting that fractional crystallization of a metallic core should have caused variations in $\delta^{57}Fe$ for both solid and liquid iron. Jordan et al. (2019) found that the Fe isotope ratio data for IIIAB irons are not consistent with a simple fractional crystallization model because there is no correlation between $\delta^{57}Fe$, based on solid/liquid fractionations similar to those obtained by Ni et al. (2020), and trace element indicators of fractional crystallization. These authors concluded that some other process, possibly evaporation, for example, must have fractionated the Fe isotopes. Ni et al. (2020) suggested that IIIAB irons represent only a fraction of the core material, as suggested previously on the basis of fractional crystallization modeling (Chabot, 2004), and that a significant fraction of the core that would be enriched in incompatible sulfur, and the isotopically light Fe conjugate to the isotopically heavy Fe in residual solids, is missing from our sample collections. Shahar and Young (2020) recently summarized these alternative interpretations of the IIIAB Fe isotope data. It is clear that understanding the processes that affected the magmatic iron meteorites and their fidelity as representatives of the cores of their parent bodies are critically important for interpreting their Fe isotope ratios, just as they are for understanding other features of these meteorites.

We will not provide a definitive assessment of the relative veracity of one model or another here. Instead, the goal is to show the essential differences between the fractional crystallization models and the impacts of these differences on interpretations of Fe isotope ratios. We conclude that, as is so often the case, the distinction comes down to assumptions about the concentration of S ([S]) in the planetesimal cores.

TRACE ELEMENTS AS TRACERS OF FRACTIONAL CRYSTALLIZATION

Trace Element Systematics

Here, we focus on Ir and Au as archetypes for compatible and incompatible trace elements, respectively, in the Fe-rich metal system. The data for the IIIAB irons are shown in a log–log plot in Fig. 1. The zero-order features of the plot are the strong suggestions of a linear trend with a negative slope and the dispersion of data along this trend. These are precisely the features expected for a suite of samples representing fractional crystallization on a log–log plot of a compatible element plotted against an incompatible element, as shown below.

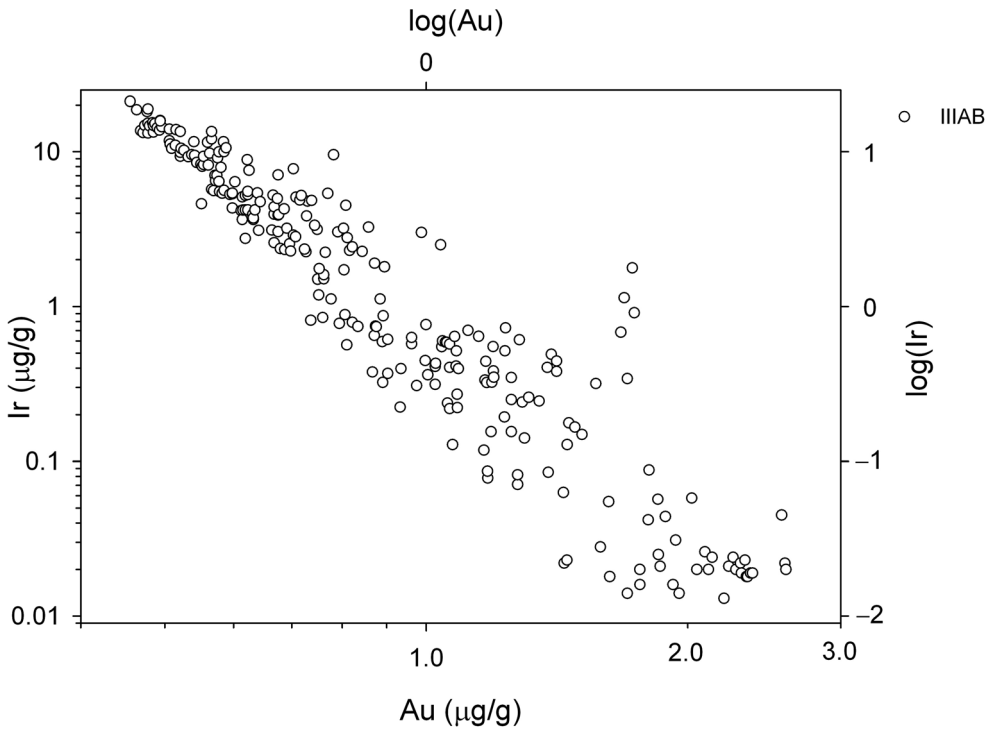

Fig. 1. IIIAB data for Ir and Au compiled by Wasson (as provided by J. T. Wasson, see Chabot & Zhang, 2021).

One can analyze the meaning of the data in Fig. 1 using the tenets of Rayleigh fractionation of trace elements in general even apart from the particulars of the models. A more or less random sampling of solids and/or melts from a suite of samples related by fractional crystallization should result in a linear trend or two parallel trends, one for liquids and one for solids, in Fig. 1. From the Rayleigh equation for the evolution of the concentration of element i in the liquid (L) with the initial concentration specified with the zero superscript, we have

$$\frac{C_i^L}{C_i^o} = F^{D_i - 1}. \tag{1}$$

where D_i is the solid/liquid distribution coefficient for element i (the ratio of the concentration of i in the solid relative to that in the liquid at equilibrium) and F is the fraction of melt remaining. This can be rearranged to yield in logarithmic form

$$\log\left(\frac{C_i^L}{C_i^o}\right) = (D_i - 1)\log(F). \tag{2}$$

The analogous equations for the solid are

$$\frac{C_i^S}{C_i^o} = D_i F^{D_i - 1}. \tag{3}$$

and

$$\log\left(\frac{C_i^S}{C_i^o}\right) = (D_i - 1)\log(D_i F). \tag{4}$$

Based on these equations, and with the simplification of invariant distribution coefficients for Ir and Au, we expect solids produced by Rayleigh fractional crystallization to produce a straight line with a negative slope in log[Ir] versus log[Au] space and coexisting liquids to produce another parallel line but offset to higher concentrations of Au. These lines would look very much like bounds on the data in Fig. 1 (Fig. 2). The slope for both lines comes from ratioing the equations for Ir and Au for the liquid:

$$\frac{\log\left(\frac{C_{\mathrm{Ir}}^L}{C_{\mathrm{Ir}}^o}\right)}{\log\left(\frac{C_{\mathrm{Au}}^L}{C_{\mathrm{Au}}^o}\right)} = \frac{(D_{\mathrm{Ir}} - 1)\log(F)}{(D_{\mathrm{Au}} - 1)\log(F)} = \frac{(D_{\mathrm{Ir}} - 1)}{(D_{\mathrm{Au}} - 1)}. \tag{5}$$

The slope is negative since $D_{\mathrm{Ir}} >> 1$ and $D_{\mathrm{Au}} < 1$. A bit of algebra shows that the offset between the melt and solid in the x axis (the log(Au) axis) should be

$$b = \frac{\log(D_{\mathrm{Au}})(D_{\mathrm{Ir}} - 1)}{s}, \tag{6}$$

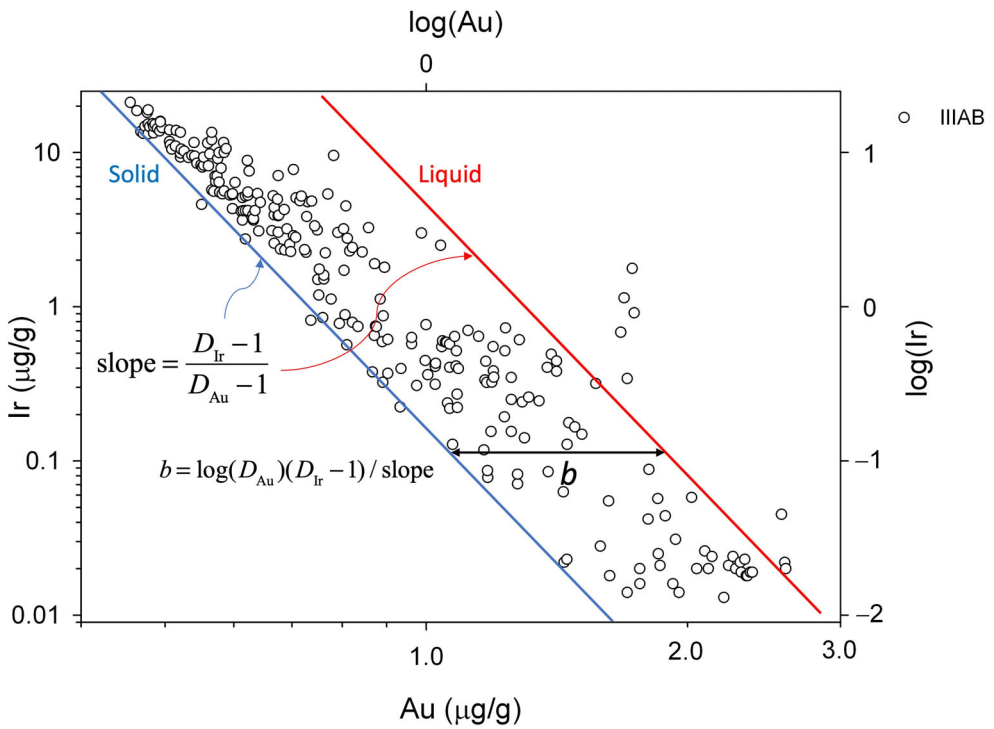

Fig. 2. Simple interpretation of IIIAB iron meteorite Ir and Au data based on the tenets of Rayleigh fractional crystallization. Open circles are IIIAB data. Model lines are described in the text.

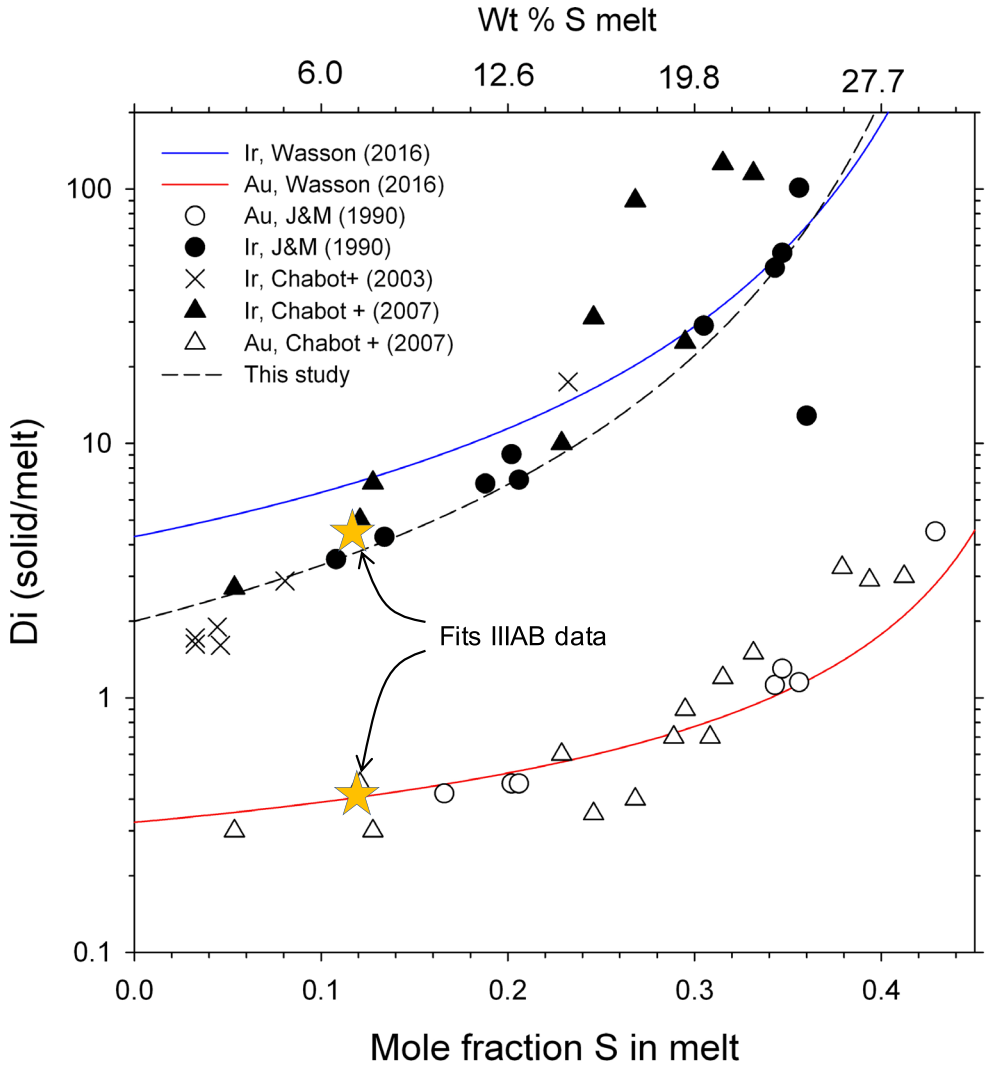

Fig. 3. Comparison of experimental data to the Wasson (2016) formulation of D_{Ir} and D_{Au} as a function of the mole fraction of S in the Fe-rich melt phase. The stars show the values consistent with the blue and red lines in Fig. 2. Measured distribution coefficients from the literature (see text) are shown for reference. The dashed curve shows an alternative fit to the D_{Ir} versus mole fraction of S data obtained by the author and resembling that from Chabot and Jones (2003).

where s is the slope from Equation 5 and b is the separation in log[Au] (Fig. 2). These relationships are shown qualitatively in Fig. 2. By measuring the rise/run in Fig. 2, using, for example, the blue line that might be plausibly interpreted as representing the solids in the system, one obtains a slope of −5.94 (e.g., [log(0.01)−log(10)]/[log(1.6)−log(0.5)]).

The simple result depicted in Fig. 2 has led many authors for decades to conclude that these meteorites represent different degrees of fractional crystallization and different mixtures of solids and melts. The success of even the most basic model for fractional crystallization in explaining the data in Fig. 2 has been the impetus for more quantitative modeling. Next, we look at specific values for the distribution coefficients to see if they are consistent with the first-order relationships shown in Fig. 2.

Wasson (2016) used the Chabot and Jones (2003) formulation for the Ir and Au distribution coefficients that evolve with composition; the distribution coefficients are not constant because of the propensity of the melt to concentrate sulfur that in turn affects the partitioning of other elements. Figure 3 shows Wasson's (2016) functions for D_{Ir} and D_{Au} variations with [S] compared with the often cited experimental data from Jones and Malvin (1990), Chabot et al. (2003), and Chabot et al. (2007). The parameterization used by these workers is log D_i = log D_o – βlog(Fe domains) where "Fe domains" refers to the Fe not bonded to the light element, in this case S, and is taken to be $(1 - 2X[S])/(1 - X[S])$ where X(S) is the mole fraction of S in the melt. For convenience, Fig. 3 shows D_i values as

functions of X(S) rather than Fe domain, as calculated using the Fe domain formulation.

The figure shows that the formulation used by Wasson in his modeling matches the experimental data with the exception of Ir at <~6 wt% S for the melt. An arguably better fit obtained by the author is shown by the dashed curve in Fig. 3. We next consider the data for D_{Ir} and D_{Au} (the points in Fig. 3) in the context of the IIIAB data and the model curves in Fig. 2.

From the experimental data for D_i values, we expect that D_{Au} should be between 0.3 and 0.4 for melt S concentrations of less than about 12 wt%. We use 0.4 as a trial value representative of relatively low S concentrations in order to investigate how this works out in the simplest possible calculation where D_i values are taken to be constant. Using our estimated slope from Fig. 2 of approximately −5.94 and the D_{Au} value of 0.4, one calculates that a D_{Ir} value of 4.5 is required to match the observed slope. Inspection of Fig. 3 shows that this value for D_{Ir} is consistent with the experimental data for a mole fraction of S in the melt of a bit more than 0.1, or roughly 7 wt%.

From this discussion, it seems that the average solid/liquid D_{Ir} and D_{Au} values of about 4.5 and 0.4, respectively, representing modest concentrations of S in the melt, explain the slopes suggested by the data in Fig. 2. What about the solid–liquid separation implied by these distribution coefficient values? Using Equation 6, we calculate that $b = \log(Au)_{liquid} - \log(Au)_{solid}$ should be ~0.23, consistent with the observed offset in [Au] for the solid and liquid from 1.6 to 2.6 μg g^{-1}, a difference of 0.21 in log units at [Ir] = 0.01, that is, as evidenced at the lower end of the envelope shown in Fig. 2. In other words, estimates for constant distribution coefficients for Ir and Au provide a self-consistent model for solid and liquid components formed by fractional crystallization as represented by the IIIAB iron meteorites using moderate concentrations of sulfur in the parental melt.

The calculations above comprise the root of the Wasson fractional crystallization trace element model for the IIIABs—fractional crystallization lines depicting the evolution of the melt and solid comprise an envelope around the great majority of the IIIAB data. The data falling between the liquid and solid lines represent mixtures of trapped melt and solid, as described by Wasson (1999, 2016). The data are seen as defining mixtures between solids (blue line in Fig. 2) and liquids (red line in Fig. 2) and the distribution coefficients need not have changed much during the crystallization process since the data appear to be fit reasonably well by linear relationships in log[Ir] versus log[Au] space. From Fig. 3, this constancy of D_i values would imply relatively low [S] in the melts in general.

The updated model used by Wasson (2016) is shown in Fig. 4. In this version, the distribution coefficients vary as depicted in Fig. 3 as the concentration of incompatible sulfur rises in the melt. In these calculations, [S] rises from an initial value of 2 wt% to a value in the most fractionated melt of near 11 wt% based on an S solid/liquid distribution coefficient of 0.005. The success of the model relies on the prescription for D_{Ir} as a function of [S] that deviates from the experiments at low concentrations of sulfur (Fig. 3). Wasson (1999) justified such deviations by arguing that fitting the IIIAB data to the simple model may be a means of extracting distribution coefficients in the face of scatter in experimental results.

Alternative Model

Chabot (2004) suggested that Wasson-like fractional crystallization models are not consistent with the experimental distribution coefficients. The argument was made that the Wasson trapped melt models were incorrect largely because their successful fit to the data in log[Ir] versus log[Au] space relied on an aberrant formulation for D_{Ir} (e.g., Fig. 3). The calculations above show that this claim is perhaps overstated. Invariant distribution coefficients for both Ir and Au required to explain the IIIAB data in the context of the fractional crystallization and trapped melt model are consistent with the experimental data (Fig. 3). A simple model like that shown above (e.g., D_i values shown by the stars in Fig. 3, yielding the lines enveloping the data in Fig. 2) matches both the IIIAB data and the experimental distribution coefficient data.

The primary difference between the model proposed by Chabot (2004), and expanded upon by Ni et al. (2020) and in this volume by Chabot and Zhang (2021), and the Wasson model is that the former authors make full use of the experimentally determined compositional dependence of the D_i values as the sulfur concentration in the melts increased by virtue of progressive crystallization. In order to arrive at a workable model, these authors invoke concentrations of S in the parental melt of about 9 wt% or greater (12 wt% in Ni et al., 2020). Concentrations of S of this magnitude are comparable to the concentrations in Fe-Ni-S components of some chondrites that range up to about 15 wt% (Scott & Kracher, 2020), but are significantly higher than bulk S concentrations in magmatic iron meteorites in general. This in turns suggest that there was an as yet unseen S-rich liquid involved in the evolution of the IIIAB irons. Referring back to the fact that the slope in the log[Ir] versus log[Au] diagram defined by solids or liquids is $(D_{Ir} - 1)/(D_{Au} - 1)$, together with the dependency of D_{Au} on [S] (Fig. 3), one can see that the negative slope in

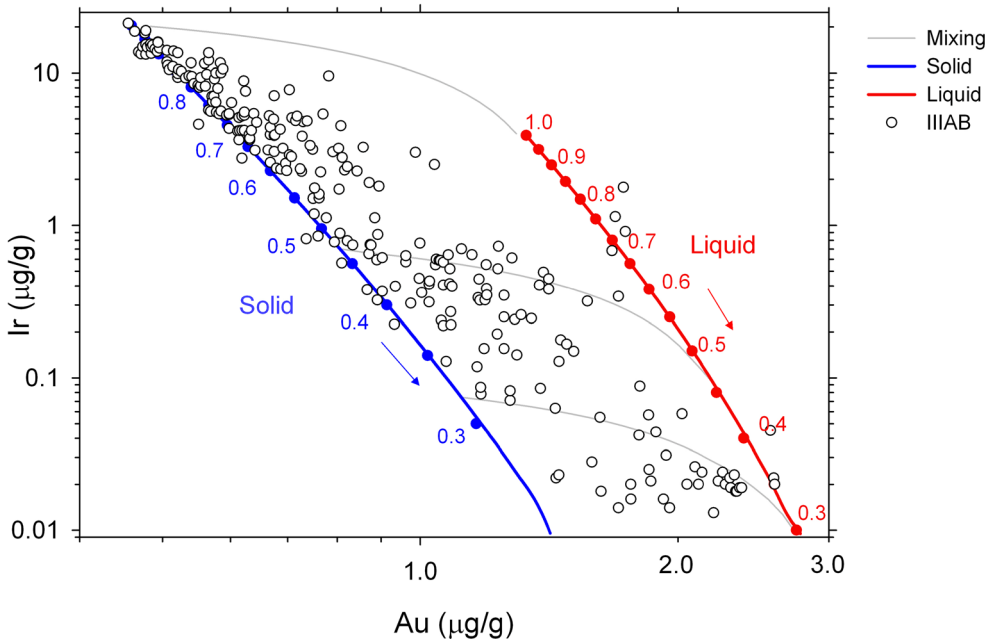

Fig. 4. The fractional crystallization and mixing model for the IIIAB iron meteorites in logarithmic [Ir] versus [Au] space according to Wasson (2016). The blue curve represents solid and the red curve coexisting liquid. Fractional amounts of liquid remaining, *F*, are indicated on both curves, and the arrows illustrate the progression with crystallization. Gray lines show representative mixing curves between solid and liquid (Wasson, 2016). Approximately 270 analyses of IIIAB meteorites are shown for comparison (Wasson, personal communication, see Chabot & Zhang, 2021). The curvature in the models at lower [Ir] values result from increasing S concentrations in the residual melt with crystallization and the effects that S has on the distribution coefficients.

log[Ir] versus log[Au] space should steepen as [S] rises because D_{Au} approaches unity as D_{Ir} increases further above 1. Chabot (2004, and in subsequent work) used the curvature in the solid side of the data envelope to infer that melt equilibrated with the solids represented by the IIIAB iron meteorites was more S rich than is indicated by simply adding up the S found in troilite inclusions.

Ni et al. (2020), described in detail by Chabot and Zhang (2021), put forward a trapped melt model that builds on the observations of Chabot (2004). In this model, the IIIAB parental melt begins with ~12 wt% S. The high concentrations of S in these evolving melts are manifested as a near vertical slope in the loci of melt compositions in log[Ir] versus log[Au] space (Fig. 5). The initial melt concentrations are set so the solid crystallizing from this melt is similar to that used in the Wasson model, coinciding with the low-[Au] edge of the IIIAB data trend in log[Ir] versus log[Au] space. Perhaps the most intriguing aspect of this model is that the IIIAB data on the high-[Au] side of the array of data, where Wasson calculates the melt to be, are interpreted as representing solidified, low-S trapped melt, with the S having been removed by crystallization of troilite. The premise is that the concentrations of the relevant siderophile trace elements will be enhanced in the Fe-rich melt simply by exclusion from the solid sulfide. The curve to the right in Fig. 5, representing the trapped melt, is calculated from the fractionated liquid using $[i]_{trapped}=[i]_{melt}/(1 - x_{troilite})$ where $x_{troilite}$ is the mass fraction of the trapped melt composed of FeS and $[i]$ is the concentration of element i in the trapped residual melt and the main mass of fractionating melt, respectively. In this interpretation, the IIIAB data in log [Ir] versus log[Au] space are bracketed by a curve representing solids formed by fractional crystallization of the parental melt on the low [Au] side of the data suite (left side in Fig. 5), and a curve representing solidified, relatively S-poor trapped liquid on the high [Au] side (right side in Fig. 5).

RELATIVE MERITS OF THE TWO MODELS

It is worth recalling that approximately constant values for D_{Ir} and D_{Au} for a parental melt sulfur concentration of about 7 wt% (the stars in Fig. 3), a reasonable median for the evolution of melts with a bulk initial [S] of 2 wt%, provide an adequate description of fractionating liquid and solid that bound the IIIAB data (e.g., Fig. 2). This underscores the fact that it is the higher [S] together with the details of changes in distribution coefficients driven by evolving

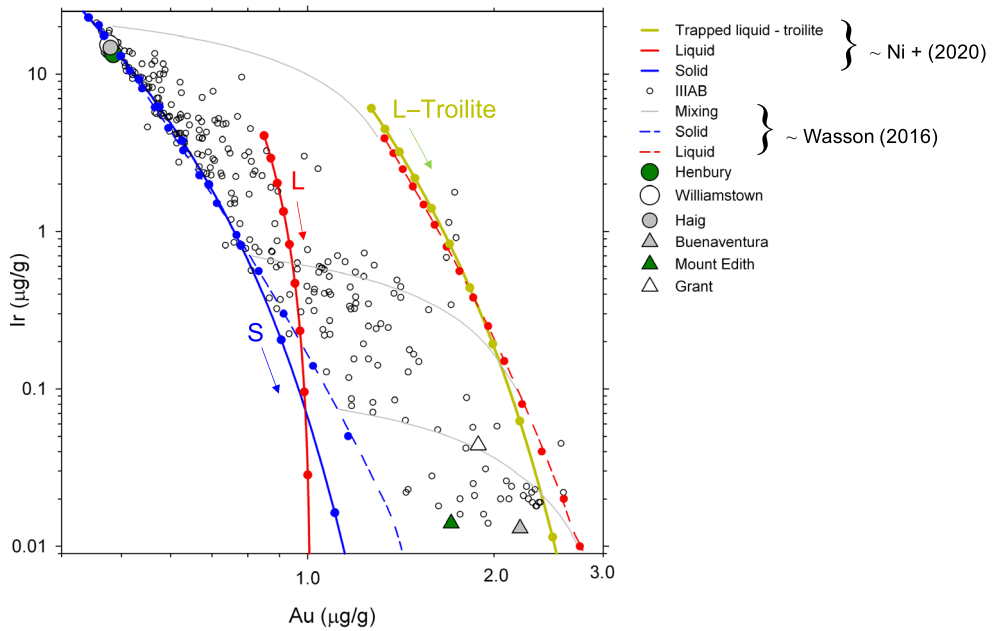

Fig. 5. IIIAB iron meteorites plotted in [Ir] versus [Au] space, with the six studied by Jordan et al. (2019) given their own symbols. The Wasson (2016) models for fractional crystallization of melt with coexisting solid are shown with the dashed curves. The curves labeled S, L, and L–troilite represent solid, liquid, and trapped liquid with troilite removed, respectively, in a version of the model put forward by Ni et al. (2020) as calculated by the author. Dots mark 0.05 increments of F starting with a maximum of $F = 1$ at the upper end of each curve. Arrows illustrate the progression with crystallization. The IIIAB data are interpreted as mixtures of solid and trapped melt in the Wasson model (gray curves) and as mixtures of solid and trapped melt that lost its S-rich troilite component in the Ni et al. (2020) model. The D_{Ir} values shown by the dashed curve in Fig. 3 were used to construct the Ni et al. (2020) model curves here.

[S] that are the important distinctions between the Wasson (2016) model and the Ni et al. (2020)/Chabot and Zhang (2021) model. The Wasson description of the IIIAB iron meteorites as mixtures of solid and liquid Fe-rich metal has to recommend it the attribute of being relatively robust. Conversely, the Ni et al. (2020)/Chabot and Zhang (2021) model offers a solution to the problem of explaining the array of IIIAB in log[Ir] versus log[Au] data while remaining faithful to the prescriptions for variations in D_i values with [S] as long as the concentration of sulfur in the parental melt is between about 12 and 15 wt%. The degree of fractionation is also more limited in the Ni et al. (2020) model, with F ranging from 1 to about 0.7 compared with variations of from 1 to <0.3 in the Wasson (2016) model. On the one hand, the Ni et al. (2020) model is very specific in constraining the nature of the bulk chemistry and evolution of the IIIAB parent body core. On the other hand, the model is less robust than simpler models and requires that the excellent fit to the data using the simple model shown in Fig. 2 is misleading. Albarede et al. (2013) described instances where the dependence of distribution coefficients on sulfur concentrations can lead to misleading trends in log–log trace element plots.

IMPLICATIONS FOR IRON ISOTOPE RATIOS IN IIIAB METEORITES

In the context of the Wasson trapped melt model, the fact that IIIAB iron meteorites with very different concentrations of Ir and Au have indistinguishable δ^{57}Fe values precludes attributing the relatively high δ^{57}Fe values to fractional crystallization. In the context of the Ni et al. (2020) model, the iron isotope ratios in IIIAB represent heavy isotope enrichment by two processes, Fe-rich solid/liquid fractionation and fractionation between Fe-rich melt and the S-rich phase (taken to be troilite) crystallizing from the S-enriched trapped melts. The Fe isotope fractionation between metal and troilite is similar to metal–silicate fractionation, favoring heavy isotopes in the Fe-rich metal phase (e.g., Chernonozhkin et al., 2016; Shahar & Young, 2020; Wang et al., 2014; Williams et al., 2006). Iron isotope fractionation between liquid and solid Fe-rich metal together with iron–troilite fractionation that also favors heavy Fe isotopes in the Fe-rich, S-poor phase, conspire to elevate δ^{57}Fe values in all but the most S-rich components that should be dominated by FeS and that have thus far evaded sampling. Since both fractionation effects favor heavy Fe isotopes in the solid

Fe-rich phase, the IIIAB meteorites are interpreted to represent only the S-poor fraction of the IIIAB parent body core. In this interpretation, the similarity in $\delta^{57}Fe$ values among these meteorites is partly serendipitous due to two different fractionation effects operating together, as shown below.

Figure 5 shows the six IIIAB samples analyzed for their Fe isotopic compositions by Jordan et al. (2019). The degree of fractionation of these samples is constrained by their concentrations of highly incompatible arsenic, As (Jordan et al., 2019). The parameter F in the Rayleigh equation is rigorously the denominator for the concentration terms relative to the initial value. For concentrations resulting from Rayleigh fractional crystallization, it is therefore the fraction of melt remaining. Assuming that the mass of As is constant in the melt due to its highly incompatible nature, the ratio of the initial concentration of As, $[As]_o$, to the concentration of As, $[As]_j$, in any sample j in a fractional crystallization sequence corresponds to $F = M_j/M_o$, the mass of melt remaining relative to the initial mass of melt. Using the [As] proxy for F, the IIIAB meteorites Buenaventura, Mount Edith, and Grant represent residual melts having experienced significant fractional crystallization. This is also evident by their positions in Fig. 5. Henbury, Williamstown, and Haig plot at the position of the initial solids in the fractionation models in Fig. 5 and so appear to represent solidified melts having experienced little to no fractional crystallization. In the context of the Wasson model, Buenaventura, Mount Edith, and Grant would be considered to be mixtures of solid and melt in the core of the parent body, both having been affected by fractional crystallization, while Henbury, Williamstown, and Haig would be considered to be solids formed from unfractionated melt. In this case, differences in $\delta^{57}Fe$ between these groups of samples are expected due to fractionation between Fe-rich solids and liquids (Fig. 6). In the context of the Ni et al. (2020) model, Buenaventura, Mount Edith, and Grant would be interpreted as being vestiges of S-poor trapped melts that were "pushed" to higher $\delta^{57}Fe$ values due to equilibration with crystallizing troilite that favors the light isotopes of Fe (Fig. 6); the liquids represented by these fractionated samples would have lost significant isotopically light iron in the form of troilite, leading to high $\delta^{57}Fe$ values.

In order to calculate the Fe isotopic consequences of fractional crystallization followed by loss of troilite from trapped melts, the same approach is used as in the case of the trace elements; the assumption is made that all S goes to the FeS component in the trapped melt. However, in the case of the isotopes, one needs to calculate the fraction of Fe comprising FeS and the fraction of Fe comprising the Fe-rich melt. Fractional crystallization removes Fe-rich solid from the melts during bulk fractional crystallization, and the measured fractionation factor between solid and metal iron is used to calculate the isotopic composition of the residual melt using the usual expression for Rayleigh fractionation: $R/R_o = F^{(\alpha-1)}$ where R is in this case the $^{57}Fe/^{54}Fe$ isotope ratio in the remaining melt, R_o is the initial ratio, and α is the solid/liquid $^{57}Fe/^{54}Fe$ fractionation factor (1.00015, from Ni et al., 2020). For isotope ratios, F in the Rayleigh equation is the abundance of the major isotope of interest relative to the initial value (Young, 2001). In the present application, $F = {}^{54}Fe/{}^{54}Fe_o$ in the melt. In the case of the S-enriched trapped melts, one adds the additional isotopic effects of equilibrating the Fe isotopes between trapped melt and troilite, resulting in the trapped melt—troilite (trapped melt "minus" troilite) curve in Fig. 6. Because progressive fractional crystallization causes the melt to become more enriched in S, and thus a higher fraction of the Fe in any trapped melt goes to the FeS phase, more and more of the isotopic effect of loss of troilite is taken up by the remaining liquid as the fraction of liquid in the system as a whole decreases. In other words, the $\delta^{57}Fe$ values of the trapped melts increase as the melts have progressively more and more sulfur in the fractionated liquids, and thus, more of the trapped Fe is partitioned to the FeS phase (Fig. 6). The mass balance expression that captures this behavior is $\delta^{57}Fe_{trapped} = \delta^{57}Fe_{melt} - x_{Fe,troilite} \times 10^3\ln(\alpha)$ where $x_{Fe,troilite}$ is the fraction of iron in the trapped melt removed as FeS (i.e., moles of Fe associated with moles of S), $\delta^{57}Fe_{melt}$ is the isotopic composition of the fractionated melt prior to the removal of troilite, and $\delta^{57}Fe_{trapped}$ is the isotopic composition of the trapped melt after the removal of troilite. Here, $10^3\ln(\alpha)$ is a good approximation to $\delta^{57}Fe_{troilite} - \delta^{57}Fe_{trapped}$. As $x_{Fe,troilite} \longrightarrow 1$, the shift in $\delta^{57}Fe$ of the trapped liquid approaches $10^3\ln(\alpha)$, and as $x_{Fe,troilite} \longrightarrow 0$, the trapped melt $\delta^{57}Fe$ value is the same as that of the residual melt from fractional crystallization of iron metal.

In the version of the S-rich trapped melt scenario presented here, based on Ni et al. (2020), the high $\delta^{57}Fe$ values relative to chondrites of the fractionated samples Buenaventura, Mount Edith, and Grant would be interpreted as being the result of extensive loss of solid Fe and FeS, resulting in high concentrations of highly incompatible elements like As, signifying low values for F, and relatively high $\delta^{57}Fe$ values. Two curves are shown in Fig. 6, one for equilibrium with troilite followed by batch removal of troilite, and the other for Rayleigh fractional loss of troilite. In order for the curves to pass through these data in Fig. 6, a relatively high value for the fractionation factor between troilite and Fe-rich metal of 0.99925 was used, corresponding to a subsolidus temperature of 900 K (data summarized by

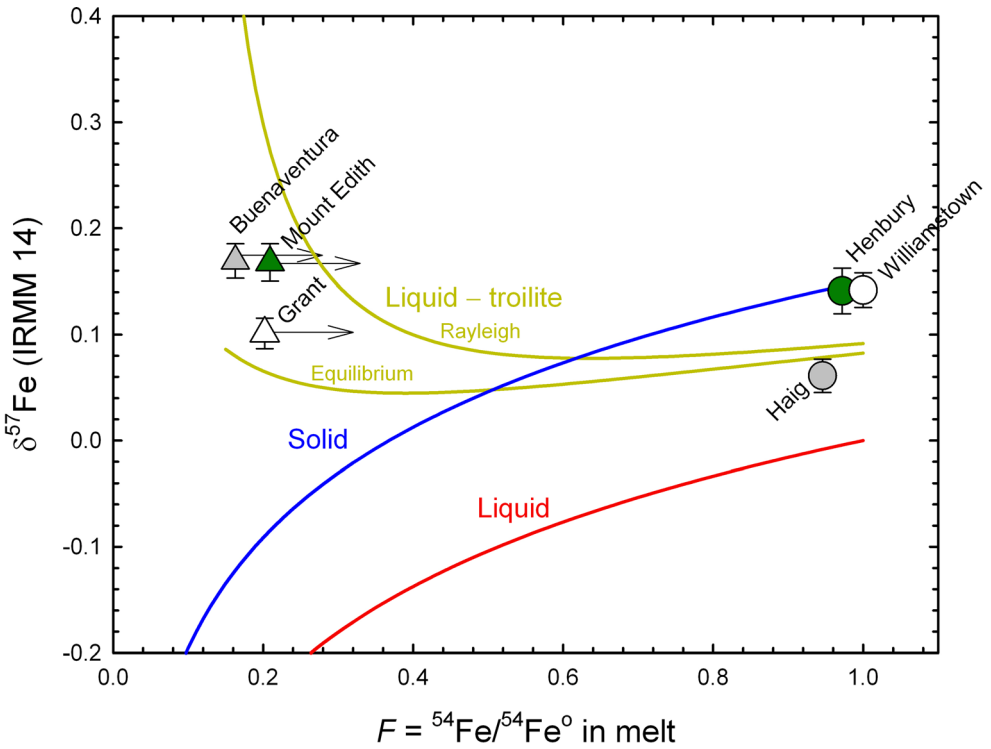

Fig. 6. Models for the fractionation of Fe isotope ratios ($^{57}Fe/^{54}Fe$) compared with data for the six IIIAB samples analyzed by Jordan et al. (2019). Arrows adjacent to the data points indicate that the *F* values are minimum values based on arsenic being perfectly incompatible. The red and blue curves labeled liquid and solid refer to solid and liquid experiencing fractional crystallization of an Fe-rich solid. The green curves labeled liquid-troilite show the effect of removal of the FeS component from a trapped melt with the isotopic composition of the liquid at the indicated value for *F*, following Ni et al. (2020). Two mechanisms of troilite removal are depicted, batch equilibrium and Rayleigh fractionation. The solid/liquid fractionation factor between solid and liquid iron used is 1.00015, consistent with the values reported by Ni et al. (2020). The troilite-Fe-rich melt fractionation is taken from that work as well, where in this case an equilibration temperature of 900 K for Fe isotopes is used (see text).

Ni et al., 2020). The maximum temperature for Fe-FeS equilibration in trapped melts capable of explaining the observed isotope ratios is about 1100 K. However, the magnitude of Fe isotope fractionation between troilite and Fe metal as a function of temperature and melt composition deserves greater attention experimentally. In addition, when comparing data to model curves in Fig. 6, it is worth pointing out that the exact positions of the fractionated samples on the abscissa of the diagram depend on the details of the partitioning of As during the fractionation process. Here, for the placement of the samples, we have assumed that As is excluded entirely from both solid iron metal and troilite in estimating *F* for these samples. To the extent that As is more compatible than this, these values for *F* are minimum values (Fig. 6). In any case, the essential conclusion from Fig. 6 is that the $\delta^{57}Fe$ values of the residual melt do not decrease with crystallization in the case of troilite removal, and this can help explain why there is no significant difference in $\delta^{57}Fe$ among this suite of IIIAB samples that differ significantly in their incompatible element concentrations.

CONCLUSIONS

The relative merits of the two interpretations of the IIIAB trace element and isotope data can be debated. The purpose here is to point out that the issues standing between the models are not as simple as differences in distribution coefficients; the salient features of the Wasson trapped melt model can be obtained using distribution coefficients consistent with experimental data. Rather, it lies with inferred bulk concentrations of S in the parental melts. The original trapped melt model of Wasson nicely explains variations in the concentrations of a number of IIIAB trace elements, but cannot accommodate large [S] and large variations in [S] and cannot explain the iron isotope ratio data. The Wasson model has the advantage that it does not rely on a significant missing component from the IIIAB core. The troilite removal model has the benefit of accommodating higher concentrations of sulfur that might be expected on the basis of comparisons with chondrite metal components, and provides solutions to some otherwise vexing trends in a number of trace

elements (Chabot & Zhang, 2021). It seems that the interpretation of the Fe isotope data in magmatic iron meteorites will come down to the initial concentration of S in the parent body cores, a persistent problem yet to be solved conclusively.

Acknowledgments—The author thanks Anat Shahar, Jabrane Labidi, Ed Scott, and Peng Ni for helpful comments during the preparation of this manuscript, and Corliss Sio and Steven Goderis for helpful reviews. The work is dedicated to Prof. John T. Wasson, a pioneer in the field of cosmochemistry and a valued colleague at UCLA.

Data Availability Statement—The data that support the findings of this study will be available in an appropriate repository once the Wasson volume is published in connection with the chapter by Chabot and Zhang.

Editorial Handling—Dr. Edward Scott

REFERENCES

Albarede, F., Bouchet, R. A., and Blichert-Toft, J. 2013. Siderophile Elements in IVA Irons and the Compaction of their Parent Asteroidal Core. *Earth and Planetary Science Letters* 362: 122–9.

Chabot, N. L. 2004. Sulfur Contents of the Parental Metallic Cores of Magmatic Iron Meteorites. *Geochimica et Cosmochimica Acta* 68: 3607–18.

Chabot, N. L., Campbell, A. J., Jones, J. H., Humayun, M., and Agee, C. B. 2003. An Experimental Test of Henry's Law in Solid Metal-Liquid Metal Systems with Implications for Iron Meteorites. *Meteoritics & Planetary Science* 38: 181–96.

Chabot, N. L. and Jones, J. H. 2003. The Parameterization of Solid Metal-Liquid Metal Partitioning of Siderophile Elements. *Meteoritics & Planetary Science* 38: 1425–36.

Chabot, N. L., Saslow, S. A., McDonough, W. F., and McCoy, T. J. 2007. The Effect of Ni on Element Partitioning During Iron Meteorite Crystallization. *Meteoritics & Planetary Science* 42: 1735–50.

Chabot, N. L. and Zhang, B. 2021. Crystallization of the IIIAB Group and a Revised Trapped Melt Model for Iron Meteorites. *Meteoritics & Planetary Science*. https://doi.org/10.1111/maps.13740.

Chernonozhkin, S. M., Goderis, S., Costas-Rodríguez, M., Clayes, P., and Vanhaecke, F. 2016. Effect of Parent Body Evolution on Equilibrium and Kinetic Isotope Fractionation: A Combined Ni and Fe Isotope Study of Iron and Stony-Iron Meteorites. *Geochimica et Cosmochimica Acta* 186: 168–88.

Esbensen, K. H., Buchwald, V. F., Malvin, D. J., and Wasson, J. T. 1982. Systematic Compositional Variations in the Cape York Iron Meteorite. *Geochimica et Cosmochimica Acta* 46: 1913–20.

Jones, J. H. and Malvin, D. J. 1990. A Nonmetal Interaction Model for the Segregation of Trace Metals During Solidification of Fe-Ni-S, Fe-Ni-P, and Fe-Ni-S-P Alloys. *Metallurgical Transactions B* 21B: 697–706.

Jordan, M. K., Tang, H., Kohl, I. E., and Young, E. D. 2019. Iron Isotope Constraints on Planetesimal Core Formation in the Early Solar System. *Geochimica et Cosmochimica Acta* 246: 461–77.

Kehm, K., Hauri, E. H., Alexander, C. M. O. D., and Carlson, R. W. 2003. High Precision Iron Isotope Measurements of Meteoritic Material by Cold Plasma ICP-MS. *Geochimica et Cosmochimica Acta* 67: 2879–91.

Lovering, J. F. 1957. Differentiation in the Iron-Nickel Core of a Parent Meteorite Body. *Geochimica et Cosmochimica Acta* 12: 238–52.

Ni, P., Chabot, N. L., Ryan, C. J., and Shahar, A. 2020. Heavy Iron Isotopes for Iron Meteorites Caused by Core Crystallization. *Nature Geoscience* 13: 611–5.

Poitrasson, F., Halliday, A. N., Lee, D.-C., Levasseur, S., and Teutsch, N. 2004. Iron Isotope Differences Between Earth, Moon, Mars and Vesta as Possible Records of Contrasted Accretion Mechanisms. *Earth and Planetary Science Letters* 223: 253–66.

Schoenberg, R. and von Blanckenburg, F. 2006. Modes of Planetary-Scale Fe Isotope Fractionation. *Earth and Planetary Science Letters* 252: 342–59.

Scott, E. R. 1977. Geochemical Relationships Between Some Pallasites and Iron Meteorites. *Mineralogical Magazine* 41: 265–72.

Scott, E. R. D. and Kracher, A. 2020. Where are the Troilite-Rich Iron Meteorites from Planetesimal Cores? 51st Lunar and Planetary Science Conference. CD-ROM.

Shahar, A. and Young, E. D. 2020. An Assessment of Iron Isotope Fractionation During Core Formation. *Chemical Geology* 554: 119800. https://doi.org/10.1016/j.chemgeo.2020.119800.

Wang, K., Savage, P. S., and Moynier, F. 2014. The Iron Isotope Composition of Enstatite Meteorites: Implications for Their Origin and the Metal/Sulfide Fe Isotopic Fractionation Factor. *Geochimica et Cosmochimica Acta* 142: 149–65.

Wasson, J. T. 1999. Trapped Melt in IIIAB Irons; Solid/Liquid Elemental Partitioning During the Fractionation of the IIIAB Magma. *Geochimica et Cosmochimica Acta* 63: 2875–89.

Wasson, J. T. 2016. Formation of the Treysa Quintet and the Main-Group Pallasites by Impact-Generated Processes in the IIIAB Asteroid. *Meteoritics & Planetary Science* 51: 773–84.

Weyer, S., Anbar, A. D., Brey, G. P., Munker, C., Mezger, K., and Woodland, A. B. 2005. Iron Isotope Fractionation During Planetary Differentiation. *Earth and Planetary Science Letters* 240: 251–65.

Williams, H. M., Markowski, A., Quitté, G., Halliday, A. N., Teutsch, N., and Levasseur, S. 2006. Fe Isotope Fractionation in Iron Meteorites: New Insights into Metal-Sulphide Segregation and Planetary Accretion. *Earth and Planetary Science Letters* 250: 486–500.

Young, E. D. 2001. Reply to Comment on 'Assessing the Implications of K Isotope Cosmochemistry for Evaporation in the Preplanetary Solar Nebula' by E. Young. *Earth and Planetary Science Letters* 192(1): 101–7.

Zhu, X. K., Guo, Y., Williams, R. J. P., O'Neil, J. R., Matthews, A., Belshaw, N. S., Canters, G. W. et al. 2002. Mass Fractionation Processes of Transition Metal Isotopes. *Earth and Planetary Science Letters* 200: 47–62.